AGU PUBLICATIONS

Geophysical Research Letters

RESEARCH LETTER
10.1002/2014GL062593

Key Points:
- Differing structural SST trends link to appreciable precipitation differences
- These differences are found in regions with high population and biodiversity
- Secular changes and natural variability in SSTs both relate to the differences

Supporting Information:
- Readme
- Figure S1
- Figure S2
- Figure S3
- Figure S4
- Figure S5
- Figure S6
- Table S1
- Text S1

Correspondence to:
B. T. Anderson,
brucea@bu.edu

Citation:
Anderson, B. T., B. R. Lintner, B. Langenbrunner, J. D. Neelin, E. Hawkins, and J. Syktus (2015), Sensitivity of terrestrial precipitation trends to the structural evolution of sea surface temperatures, *Geophys. Res. Lett.*, *42*, 1190–1196, doi:10.1002/2014GL062593.

Received 20 NOV 2014
Accepted 18 JAN 2015
Accepted article online 23 JAN 2015
Published online 18 FEB 2015

Sensitivity of terrestrial precipitation trends to the structural evolution of sea surface temperatures

Bruce T. Anderson[1,2], Benjamin R. Lintner[3], Baird Langenbrunner[4], J. David Neelin[4], Ed Hawkins[5], and Jozef Syktus[6]

[1]Department of Earth and Environment, Boston University, Boston, Massachusetts, USA, [2]The Frederick S. Pardee Center for the Study of the Longer-Range Future, Boston University, Boston, Massachusetts, USA, [3]Department of Environmental Sciences, Rutgers, State University of New Jersey, New Brunswick, New Jersey, USA, [4]Department of Atmospheric and Oceanic Sciences, University of California, Los Angeles, California, USA, [5]National Centre for Atmospheric Science, Department of Meteorology, University of Reading, Reading, UK, [6]Department of Science, Information Technology, Innovation and the Arts, University of Queensland, Brisbane, Queensland, Australia

Abstract Pronounced intermodel differences in the projected response of land surface precipitation (LSP) to future anthropogenic forcing remain in the Coupled Model Intercomparison Project Phase 5 model integrations. A large fraction of the intermodel spread in projected LSP trends is demonstrated here to be associated with systematic differences in simulated sea surface temperature (SST) trends, especially the representation of changes in (i) the interhemispheric SST gradient and (ii) the tropical Pacific SSTs. By contrast, intermodel differences in global mean SST, representative of differing global climate sensitivities, exert limited systematic influence on LSP patterns. These results highlight the importance to regional terrestrial precipitation changes of properly simulating the spatial distribution of large-scale, remote changes as reflected in the SST response to increasing greenhouse gases. Moreover, they provide guidance regarding which region-specific precipitation projections may be potentially better constrained for use in climate change impact assessments.

1. Introduction

Projected changes in regional land surface precipitation (LSP) frequency, intensity, and duration—which in certain locations show little intermodel consistency in even their sign—are considered among the least robust signatures of anthropogenic climate forcing [*Allen and Ingram*, 2002; *Murphy et al.*, 2004; *Neelin et al.*, 2006]. Previous studies have examined the influence of simulated land-atmosphere coupling [*Seneviratne et al.*, 2010], internal variability [*Sorteberg and Kvamsto*, 2006; *Deser et al.*, 2012a], dynamics [*Woollings*, 2010], and physics [*Piani et al.*, 2007] on intermodel variations in terrestrial precipitation trends. Despite the well-known influences of ocean processes upon regional- to global-scale precipitation variations across multiple timescales [*Giannini et al.*, 2003; *Schubert et al.*, 2004; *Meehl and Hu*, 2006], and upon oceanic precipitation in particular [*Ma and Xie*, 2013; *Frierson et al.*, 2013], the relationship between intermodel differences in projected sea surface temperature (SST) and regional LSP trends has not yet been well determined.

Here the goal is to examine whether systematic intermodel differences in the secular (i.e., long-term, nonperiodic) changes to the ocean state (in contrast to internal or natural variability) have leading associated patterns of intermodel variability in projected terrestrial (i.e., land surface) precipitation trends in the latest generation of Coupled Model Intercomparison Project Phase 5 (CMIP5) models [*Taylor et al.*, 2012]. In describing these relationships, we are careful to avoid implying that SST has a causal role because on climate change timescales the SSTs adjust to surface heat flux equilibrium in concert with the atmosphere column (with the exception of regions influenced by changes in ocean heat transport [e.g., *Chou et al.*, 2006]). Clearer insights on such causal mechanisms—which, in fact, may be quite limited [*He et al.*, 2014]—are only obtained through energy budget considerations [e.g., *Kang and Held*, 2012]. Nonetheless, SST remains a useful diagnostic variable for the present aim: identification of remote influences on intermodel differences in LSP, whether via tropical ocean to land influences akin to El Niño–Southern Oscillation (ENSO) teleconnections (for which SSTs play an active role) and/or local- to global-scale changes in energy budgets (for which SSTs play a more passive role) [e.g., *Kang et al.*, 2009; *Frierson and Hwang*, 2012; *Frierson et al.*, 2013; *He et al.*, 2014].

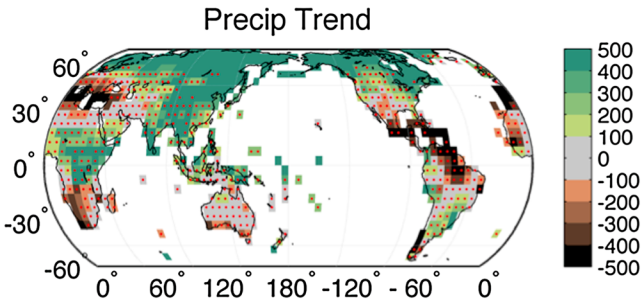

Figure 1. Multimodel mean precipitation trend estimate based upon 18 CMIP5 model simulations forced by the RCP8.5 scenario for the period 2006–2100. Multimodel mean derived from the 18 normalized precipitation trend values at each grid point, defined as the difference in the linearly interpolated 20 year mean precipitation values between the last 20 year period and first 20 year period and normalized by the standard deviation of nonoverlapping 20 year means taken from the preindustrial control run of the given model at the given grid point. Units: (%). Red dots indicate grids in which the normalized trends do *not* (i) exceed 2 standard deviations of internal variability (approximately equivalent to $\pm\sqrt{2} \times 200\%$) or (ii) do not show 90% agreement in the sign of the change—the IPCC standard criteria representing large change with high model agreement.

2. Data and Methods

For this study, we use data from CMIP5 simulations forced by the Representative Concentration Pathway (RCP) 8.5, which imposes an effective 8.5 W/m^2 forcing by the year 2100. Output from one ensemble member from eighteen (18) models for the period 2006–2100 is used (listed in supporting information Table S1). The data analyzed comprise 20 year running mean values of LSP and 20 year running mean values of SSTs (supporting information). In order to evaluate intermodel trend differences against model simulated internal variability, we further analyze (1) a 1000 year preindustrial control run; i.e., greenhouse gas forcing is prescribed to preindustrial levels, of the Community Climate System Model version 4 (CCSM4; model specifications can be found in *Gent et al.* [2011]) generated as part of CMIP5; and (2) 30 simulations of a single model (the CSIRO-Mk3.6.0 [*Rotstayn et al.*, 2012]) forced by the RCP8.5 scenario.

To quantify the intermodel differences in structural LSP trends and their relation to intermodel differences in SSTs, we perform a "Principal Uncertainty Pattern" (PUP) [*Langenbrunner et al.*, 2013] analysis utilizing both empirical orthogonal function (EOF) analysis and Canonical Correlation Analysis (CCA). Generically, EOF analysis is a univariate variance decomposition algorithm designed to maximize the variance explained by a given mode of variability within a specific data set, while CCA is a multivariate regression algorithm designed to maximize the correlation between the modes of variability from different data sets [*Bretherton et al.*, 1992; *Barnett and Preisendorfer*, 1987; *Graham et al.*, 1987; *Cherry*, 1996; *Anderson*, 2003]. Similar to previous intermodel and intramodel analyses [e.g., *Deser et al.*, 2012a; *Ma and Xie*, 2013], variance/correlation is not calculated across time, t, but across models, m. Utilizing the EOF algorithm (see supporting information) we obtain a set of principal component (PC) model weightings that explain the greatest amount of variability in intermodel SST trend differences, $\Delta T(x_2, m)$. By contrast, utilizing the CCA algorithm (see supporting information) we obtain a set of canonical factor (CF) model weightings that isolate the highest correlated modes of variability between intermodel LSP trend differences, $\Delta P(x_1, m)$, and SST trend differences, $\Delta T(x_2, m)$. Here $\Delta P(x_1, m)$ is the linear trend of the LSP, as defined according to the standard CMIP5 protocol for trend analysis (see supporting information), normalized by the standard deviation of nonoverlapping 20 year means taken from the preindustrial control run of the given model, m, at the given grid point, x_1, so as to represent the change relative to low-frequency internal variability within the given model at the given grid point (hereafter the normalized LSP trends). $\Delta T(x_2, m)$ is the linear trend of the SSTs, normalized by the standard deviation of the intermodel trends at a given grid point, x_2 (which in the model-index domain is equivalent to standardizing in the time domain). All model data have been interpolated to a common $5° \times 5°$ grid.

3. Results

We first illustrate the multimodel mean terrestrial precipitation trends at each grid point based upon 20 year running mean values of normalized LSP (Figure 1). In many places, LSP trends exceed (1σ) decadal-scale variability by the end of 21st century; however, uncertainty persists over broad areas in which the Intergovernmental Panel on Climate Change (IPCC) standard for "large change with high model agreement" remains unmet [*Intergovernmental Panel on Climate Change* (*IPCC*), 2013], in agreement with previous studies of both intermodel and intramodel uncertainty in precipitation trends [*Deser et al.*, 2012a].

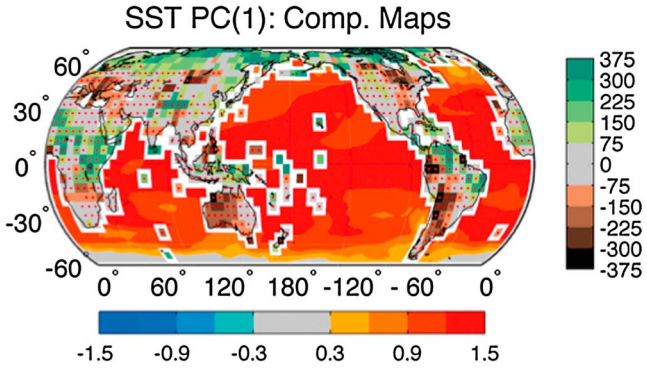

Figure 2. Green/brown shading: intermodel differences in normalized precipitation trends (as defined in Figure 1) based upon the difference in the composite mean fields for the three models with the largest positive and largest negative normalized model weightings for the first principal component (PC) of intermodel sea surface temperature (SST) trend differences—see supporting information Figure S1b for respective models used in the composite mean. Units: (%). Red dots are same as in Figure 1 and serve as reference for regions with persistent intermodel differences in precipitation trends. Shading interval given by color bar to the right. Red/blue shading: intermodel differences in normalized SST trends based upon the difference in the composite mean fields for the same set of three positive and three negative models. Values are unitless. Shading interval given by legend at bottom.

Previous work [e.g., *Ma and Xie*, 2013] has shown that intermodel variability in oceanic precipitation trends is determined in part by the magnitude of the mean SST trend within a given model, as well as by the spatial structure of that trend. To assess whether similar behavior holds for LSP, the leading mode of intermodel SST variability, as determined via EOF analysis, is isolated. Using the PC model weights, we then calculate the composite mean intermodel differences in LSP and SST trends between the three models with the most positive and the most negative weights (Figure 2); the corresponding model weights along with the full regression of the intermodel differences in LSP and SST trends on these weights are shown in the supporting information Figure S1. Overall, the leading mode of SST trend variability is positive everywhere, indicating that the leading PC of intermodel SST differences is associated with global mean SST increases (supporting information Figure S2). The largest related LSP changes occur over Australia, South America, the Horn of Africa, and the Arctic. Elsewhere, this relationship is relatively weak and sparse, as compared with the leading modes of covariability (see below).

Next we examine the leading two modes of covariability associated with systematic differences in the modeled LSP and SST trends, as determined via CCA. The composite mean intermodel difference maps for LSP and SST trends between the three models with the most positive and the most negative CF weights are shown in Figure 3; the corresponding model weights along with the full regression of the intermodel differences in LSP and SST trends on these weights are shown in supporting information Figure S3 (see also Figures 4a and 4c). Broadly, the leading mode of covariability (Figure 3a) involves intermodel differences in LSP trends over West Africa, East and Southeast Asia, and Brazil related to intermodel differences in interhemispheric SST gradient trends resulting from large-scale differences in SST trends between hemispheres (supporting information Figure S4a), with decreased LSP trends in the colder hemisphere reminiscent of high-latitude ocean circulation and/or energy budget impacts on low-latitude precipitation (supporting information Figure S4b), as noted in prior studies [e.g., *Kang et al.*, 2009; *Frierson and Hwang*, 2012; *Frierson et al.*, 2013; *Seo et al.*, 2014]. The second mode of covariability (Figure 3b) involves intermodel differences in LSP trends over Indonesia, the Amazon, the southern portion of North America, and the Sahel related to intermodel differences in SST trends across the Pacific Ocean basin, with additional intermodel differences over the North Atlantic as well as the Indian Ocean. Based upon the magnitude of the LSP differences associated with these two CFs, the structural uncertainties in SST trends (shown here) relate more to intermodel differences in regional LSP trend variations (~25% variance explained) than the overall degree of ocean warming itself (cf. ~8% variance explained—Figure 2).

We further seek modes of natural variability—which are large contributors to intramodel differences in regional circulation (and precipitation) trends [*Deser et al.*, 2012a]—that could explain intermodel differences in the projected SST trends. Using output from a 1000 year preindustrial control simulation of CCSM4, we first calculate low-frequency time series using 20 year running mean values of SSTs and LSP at each grid point, as we did with the RCP8.5 data analyzed above. We then perform a pattern correlation of the low-frequency SST variations with the CF SST maps and regress the low-frequency SST and LSP variations found within the preindustrial control simulation on the resulting time series (Figure 4). Overall, the first CF pattern of intermodel differences in SST trends projects only weakly onto low-frequency internal variability within the control

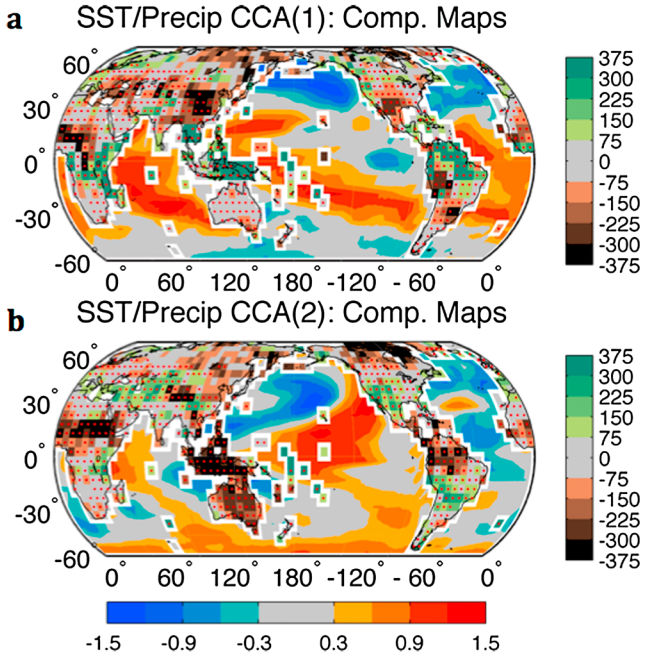

Figure 3. (a) Green/brown shading: intermodel differences in normalized precipitation trends (as defined in Figure 1) based upon the difference in the composite mean fields for the three models with the largest positive and largest negative normalized sea surface temperature (SST) model weightings associated with the first Canonical Correlation Analysis (CCA) mode of coupled intermodel trend differences—see text. See supporting information Figure S3b for respective models used in composite. Units: (%). Red dots are same as in Figure 1 and serve as reference for regions with persistent intermodel differences in precipitation trends. Shading interval given by color bar to the right. Red/blue shading: intermodel differences in normalized SST trends based upon the difference in the composite mean fields for the same set of three positive and three negative models. Values are unitless. Shading interval given by legend at bottom. (b) Same as Figure 3a except for the composite mean fields associated with the second CCA mode of coupled intermodel trend differences; see supporting information Figure S3d for respective models used in composite.

simulation's SST evolution (Figure 4b); given this weak projection on SST variability, the LSP response is also substantially reduced.

These results suggest that the first CF pattern of intermodel differences in SST and LSP trends is not related strongly to natural modes of low-frequency internal variability in the ocean but instead to intermodel differences in the secular changes of the ocean state itself. Hypothetically, intermodel differences in the applied radiative forcing—specifically that associated with short-lived aerosol loadings—could potentially account for this interhemispheric contrast. Here we note the recent work of *Xie et al*. [2013] in which the historic ensemble of CMIP5 simulations was analyzed with respect to aerosol forcing, revealing some similarity to the spatial patterns evident here (cf. Figure 2a from *Xie et al*. [2013] and Figure 4). However, preliminary examination of the intermodel differences in clear-sky shortwave radiation changes (supporting information Figure S5) suggests little if any link to downwelling shortwave radiation at the surface (supporting information Figure S5c), which would be representative of intermodel differences induced by changes in radiation transmission and absorption associated with altered chemical composition; instead, intermodel differences in clear-sky shortwave cooling in the Northern Hemisphere seem to be largely confined to the land surfaces (supporting information Figures S5a and S5b) suggesting a potentially more prominent role of ice-albedo feedbacks as a contributor to the intermodel differences in the interhemispheric temperature gradient (as noted in other contexts by *Chiang and Bitz* [2005]). Clearly, a more detailed analysis of the oceanic, terrestrial, and atmospheric energy budgets will be required to elucidate the processes involved.

By contrast, the second CF pattern of intermodel differences in SST trends appears to project onto the low-frequency internal variability of the El Niño-Southern Oscillation (ENSO) or the broader Interdecadal Pacific Oscillation within the control simulation (cf. Figures 4d and 20a from *Deser et al*. [2012b], both of which are based upon output from the CCSM4). However, with the exception of Indonesia and possibly the Sahel, the corresponding LSP variations are substantially reduced in the control simulation compared with those for the intermodel trends. As such, it appears that the second leading mode of intermodel SST/LSP covariability is related to intermodel differences in the evolution of the base state of the Pacific Ocean. These differences in model evolution could be the result of either secular changes of the ocean itself or low-frequency internal variations of the ocean/atmosphere system within the independent model runs. In either case, the spatial form of the SST anomaly is reasonably colocated with areas that influence both the climatology and natural variability of LSP and as such may be an indicator for an active role of SSTs in generating intermodel LSP differences, rather than simply being a passive participant in surface heat flux balance response.

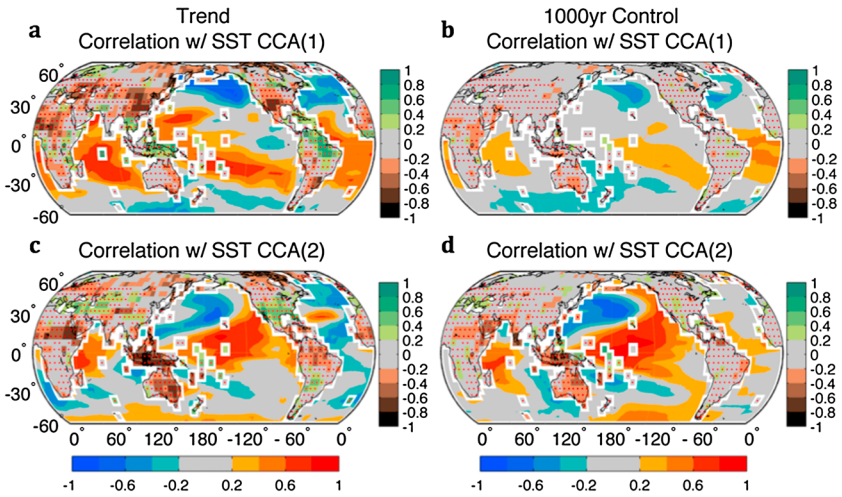

Figure 4. Projections of intermodel differences in sea surface temperature (SST) and land surface precipitation (LSP) trends onto low-frequency modes of natural variability. (a) Red/blue shading: intermodel differences in SST trends correlated with the normalized SST model weightings for the first CCA mode of coupled intermodel trend differences—see text. Values are unitless. Shading interval given by color bar at bottom. Green/brown shading: intermodel differences in normalized precipitation trends (as defined in Figure 1), correlated with the normalized SST model weightings for the first CCA mode of coupled intermodel trend differences. Values are unitless. Red dots are same as in Figure 1 and serve as reference for regions with persistent intermodel differences in precipitation trends. Shading interval given by color bar to the right. (b) Twenty year running mean values in SSTs (red/blue) and precipitation (green/brown) from the 1000 year preindustrial control simulation, correlated with the time series generated by performing a year-to-year spatial correlation of the SST anomaly map in Figure 4a with the 20 year running mean SST anomaly maps from the preindustrial control simulation. Units/values are the same as in Figure 4a. (c, d) Same as Figures 4a and 4b except for second CCA mode of coupled intermodel trend differences.

As a further check to determine whether modes of natural variability contribute to the leading modes of intermodel differences in ocean-related LSP trends, we perform the CCA utilizing LSP and SST trends from multiple (30) realizations of a single model (the CSIRO-Mk3.6.0). The leading mode of covariability across the 30 realizations of this model (supporting information Figure S6a) manifests differences in LSP trends over the Indo-Australian monsoon region, the Amazon, and western Africa coupled to differences in SST trends across the Pacific Ocean basin, as well as the Indian and North Atlantic Oceans. Broadly speaking, this behavior mirrors the second leading mode of intermodel differences in ocean-influenced LSP trends, albeit with region-specific differences, e.g., a lack of precipitation deficits in Asia and surpluses in North America. This similarity suggests that low-frequency internal variations of the ocean/atmosphere system within independent model runs—here again related to the base state of the Pacific Ocean—can contribute substantially to intermodel differences in LSP trends by the end of the 21st century.

By contrast, the second leading mode of covariability (supporting information Figure S6b) involves relatively weak within-model differences in LSP trends, mainly over parts of the Amazon and the Boreal North related to within-model differences in SST trends across all three ocean basins. This SST structure is qualitatively similar to that associated with intermodel differences in global mean SST increases (cf. Figure 2) and captures within-model variability in the global mean temperature trend and its relatively weak and sparse relationship with LSP, similar to that found in the intermodel results. Further, none of the leading modes of covariability show robust within-model differences in interhemispheric SST gradient trends; in line with the weak, low-frequency internal variability revealed by the 1000 year preindustrial control run analysis, these results suggest that the first CF pattern of intermodel differences in SST and LSP trends arises from intermodel differences in the secular changes of the ocean state itself, not natural modes of low-frequency oceanic variability.

4. Summary

Variations and trends in land surface precipitation (LSP) have important consequences for local and regional adaptation and planning activities [*Alley et al.*, 2003; *Giorgi*, 2005]; propensity for drought and flooding [*Entekhabi et al.*, 2010]; nonlinear climate feedbacks, particularly with regard to extreme temperatures

[*Seneviratne et al*., 2006; *Lorenz et al*., 2010]; regional- and continental-scale carbon fluxes [*St. Claire et al*., 2009; *Van Der Molen* et al., 2011]; and discontinuous transitions between ecological regimes [e.g., *Higgins et al*., 2002]. Unfortunately, many terrestrial regions show little intermodel and intramodel consistency in the response of LSP to increased anthropogenic emissions of radiatively active chemical constituents such as carbon dioxide and other heat-trapping gases over the course of this century [*Anderson et al*., 2009; *Deser et al*., 2012a; *IPCC*, 2013].

To better characterize sources of this regional inconsistency, we have performed a multivariate Principal Uncertainty Pattern (PUP) analysis relating intermodel differences in LSP trends to intermodel differences in sea surface temperature (SST) trends. Unlike for oceanic precipitation—particularly in the tropics where the "warmer-get-richer" mechanism amplifies the SST-induced precipitation response in warmer models and dampens it in colder models [*Ma and Xie*, 2013]—the magnitude of mean SST trends in response to intermodel differences in global climate sensitivities is not a predominant driver of LSP trend differences. Instead, the most prominent patterns of intermodel differences in coupled LSP and SST trends involve trends in (i) the interhemispheric SST gradient and (ii) the distribution of tropical Pacific SSTs. The first, which is related to intermodel differences in LSP trends over broad swaths of the globe—including West Africa, East and Southeast Asia, and Brazil—projects only weakly onto low-frequency internal variability of the ocean, in either preindustrial or future climate change scenarios. Hence, intermodel differences in LSP trends in these regions are most likely related to systematic differences in the models' structural representation of processes over broad regions that are reflected in secular SST changes, such as remote energy budget changes. Projections of the end-of-century response of precipitation in these land regions may thus potentially be improved through better constrained estimates of interhemispheric responses to anthropogenic forcing. By contrast, the second SST difference pattern—which is related to intermodel differences in land surface precipitation trends over Indonesia, the Amazon, the southern portion of North America, and the Sahel—does project onto low-frequency internal variations of the ocean. The spatial pattern of this mode is suggestive of an active oceanic influence, but the similarity to patterns of natural variability also increases the requirements for distinguishing projected precipitation responses to greenhouse gas forcings in these regions. Planning and adaptation strategies for these regions should account for this additional source of uncertainty [e.g., *Lempert et al*., 2004].

Acknowledgments

B.T.A. acknowledges support of Department of Energy grant DE-SC0004975. B.R.L. acknowledges support of National Science Foundation grant NSF-AGS-1312865. E.H. is funded by the UK National Environment Research Council. J.D.N. and B.L. acknowledge support of NSF AGS-1102838, NOAA NA11OAR4310099, and NOAA NA14OAR4310274. We acknowledge the World Climate Research Programme's Working Group on Coupled Modelling, which is responsible for CMIP, and we thank the climate modeling groups (listed in Table S1 in the supporting information) for producing and making available their model output. For CMIP the U.S. Department of Energy's Program for Climate Model Diagnosis and Intercomparison provides coordinating support and leads development of software infrastructure in partnership with the Global Organization for Earth System Science Portals. To obtain model simulations of historical and projected temperatures from the Coupled Model Intercomparison Project 5 (CMIP5) multimodel ensemble used in this study, please see http://pcmdi9.llnl.gov/esgf-web-fe/.

The Editor thanks two anonymous reviewers for their assistance in evaluating this paper.

References

Allen, M. R., and W. J. Ingram (2002), Constraints on future changes in climate and the hydrologic cycle, *Nature*, *419*, 224–232.

Alley, R. B., et al. (2003), Abrupt climate change, *Science*, *299*, 2005–2010, doi:10.1126/science.1081056.

Anderson, B. T. (2003), Tropical Pacific sea-surface temperatures and preceding sea-level pressure anomalies in the subtropical North Pacific, *J. Geophys. Res.*, *108*(D23), 4732, doi:10.1029/2003JD003805.

Anderson, B. T., C. Reifen, and R. Toumi (2009), Consistency in global climate change model predictions of regional precipitation trends, *Earth Interact.*, *13*, 1–23, doi:10.1175/2009EI273.1.

Barnett, T. P., and R. Preisendorfer (1987), Origins and levels of monthly and seasonal forecast skill for United States surface air temperatures determined by canonical correlation analysis, *Mon. Weather Rev.*, *15*, 1825–1850.

Bretherton, C. S., C. Smith, and J. M. Wallace (1992), An intercomparison of methods for finding coupled patterns in climate data, *J. Clim.*, *5*, 541–560.

Cherry, S. (1996), Singular value decomposition analysis and canonical correlation analysis, *J. Clim.*, *9*, 2003–2009.

Chiang, J. C., and C. M. Bitz (2005), Influence of high latitude ice cover on the marine intertropical convergence zone, *Clim. Dyn.*, *25*, 477–496, doi:10.1007/s00382-005-0040-5.

Chou, C., J. D. Neelin, J.-Y. Tu, and C.-T. Chen (2006), Regional tropical precipitation change mechanisms in ECHAM4/OPYC3 under global warming, *J. Clim.*, *19*(17), 4207–4223, doi:10.1175/JCLI3858.1.

Deser, C., A. Phillips, V. Bourdette, and H. Teng (2012a), Uncertainty in climate change projections: The role of internal variability, *Clim. Dyn.*, *38*, 527–546.

Deser, C., A. S. Phillips, R. A. Tomas, Y. M. Okumura, M. A. Alexander, A. Capotondi, J. D. Scott, Y.-O. Kwon, and M. Ohba (2012b), ENSO and Pacific decadal variability in the Community Climate System Model version 4, *J. Clim.*, *25*, 2622–2651, doi:10.1175/JCLI-D-11-00301.1.

Entekhabi, D., et al. (2010), The soil moisture active passive (SMAP) mission, *Proc. IEEE*, *98*, 704–716.

Frierson, D. M. W., and Y.-T. Hwang (2012), Extratropical influence on ITCZ shifts in slab ocean simulations of global warming, *J. Clim.*, *25*, 720–733, doi:10.1175/JCLI-D-11-00116.1.

Frierson, D. M. W., Y.-T. Hwang, N. S. Fučkar, R. Seager, S. M. Kang, A. Donohoe, E. A. Maroon, X. Liu, and D. S. Battisti (2013), Contribution of ocean overturning circulation to tropical rainfall peak in the Northern Hemisphere, *Nat. Geosci.*, *6*, 940–944, doi:10.1038/ngeo1987.

Gent, P. R., et al. (2011), The Community Climate System Model version 4, *J. Clim.*, *24*, 4973–4991.

Giannini, A., R. Saravanan, and P. Chang (2003), Oceanic forcing of Sahel rainfall on interannual to interdecadal time scales, *Science*, *302*, 1027–1030.

Giorgi, F. (2005), Climate change prediction, *Clim. Change*, *73*, 239–265.

Graham, N. E., J. Michaelsen, and T. P. Barnett (1987), An investigation of the El Niño-Southern Oscillation cycle with statistical models: 1. Predictor field characteristics, *J. Geophys. Res.*, *92*, 14,251–14,270, doi:10.1029/JC092iC13p14251.

He, J., B. J. Soden, and B. Kirtman (2014), The robustness of the atmospheric circulation and precipitation response to future anthropogenic surface warming, *Geophys. Res. Lett.*, *41*, 2614–2622, doi:10.1002/2014GL059435.

Higgins, P. A. T., M. D. Mastrandrea, and S. H. Schneider (2002), Dynamics of climate and ecosystem coupling: Abrupt changes and multiple equilibria, *Philos. Trans. R. Soc. London, Ser. B*, *357*, 647–655.

Intergovernmental Panel on Climate Change (IPCC) (2013), *Climate Change 2013: The Physical Science Basis. Contribution of Working Group I to the Fifth Assessment Report of the Intergovernmental Panel on Climate Change*, edited by T. F. Stocker et al., 1535 pp., Cambridge Univ. Press, Cambridge, U. K., and New York.

Kang, S. M., and I. M. Held (2012), Tropical precipitation, SSTs and the surface energy budget: A zonally symmetric perspective, *Clim. Dyn.*, *38*, 1917–1924, doi:10.1007/s00382-011-1048-7.

Kang, S. M., D. M. W. Frierson, and I. M. Held (2009), The tropical response to extratropical thermal forcing in an idealized GCM: The importance of radiative feedbacks and convective parameterization, *J. Atmos. Sci.*, *66*, 2812–2827, doi:10.1175/2009JAS2924.1.

Langenbrunner, B., J. D. Neelin, and B. T. Anderson (2013), Principal uncertainty patterns in precipitation among CMIP5 models: Dominant modes of intermodel disagreement in precipitation climatologies and projected change patterns, 2013 Fall Meeting, AGU, San Francisco, Calif.

Lempert, R., N. Nakicenovic, D. Sarewitz, and M. Schlesinger (2004), Characterizing climate-change uncertainties for decision-makers, *Clim. Change*, *65*, 1–9, doi:10.1023/B:CLIM.0000037561.75281.b3.

Lorenz, R., E. B. Jaeger, and S. I. Seneviratne (2010), Persistence of heat waves and its link to soil moisture memory, *Geophys. Res. Lett.*, *37*, L09703, doi:10.1029/2010GL042764.

Ma, J., and S.-P. Xie (2013), Regional patterns of sea surface temperature change: A source of uncertainty in future projections of precipitation and atmospheric circulation, *J. Clim.*, *26*, 2482–2501.

Meehl, G. A., and A. X. Hu (2006), Megadroughts in the Indian monsoon region and southwest North America and a mechanism for associated multidecadal Pacific sea surface temperature anomalies, *J. Clim.*, *19*, 1605–1623.

Murphy, J. M., D. M. H. Sexton, D. N. Barnett, G. S. Jones, M. J. Webb, M. Collins, and D. A. Stainforth (2004), Quantification of modeling uncertainties in a large ensemble of climate change simulations, *Nature*, *430*, 768–772.

Neelin, J. D., M. Munnich, H. Su, J. E. Meyerson, and C. E. Holloway (2006), Tropical drying trends in global warming models and observations, *Proc. Natl. Acad. Sci. U.S.A.*, *103*, 6110–6115, doi:10.1073/pnas.0601798103.

Piani, C., B. Sanderson, F. Giorgi, D. J. Frame, C. Christensen, and M. R. Allen (2007), Regional probabilistic climate forecasts from a multithousand, multimodel ensemble of simulations, *J. Geophys. Res.*, *112*, D24108, doi:10.1029/2007JD008712.

Rotstayn, L. D., S. J. Jeffrey, M. A. Collier, S. M. Dravitzki, A. C. Hirst, J. I. Syktus, and K. K. Wong (2012), Aerosol- and greenhouse gas-induced changes in summer rainfall and circulation in the Australasian region: A study using single-forcing climate simulations, *Atmos. Chem. Phys.*, *12*, 6377–6404, doi:10.5194/acp-12-6377-2012.

Schubert, S. D., M. J. Suarez, P. J. Pegion, R. D. Koster, and J. T. Bacmeister (2004), On the cause of the 1930s Dust Bowl, *Science*, *303*, 1855–1859.

Seneviratne, S. I., D. Lüthi, M. Litschi, and C. Schär (2006), Land-atmosphere coupling and climate change in Europe, *Nature*, *443*, 205–209.

Seneviratne, S. I., T. Corti, E. L. Davin, M. Hirschi, E. B. Jaeger, I. Lehner, B. Orlowsky, and A. J. Teuling (2010), Investigating soil moisture-climate interactions in a changing climate: A review, *Earth Sci. Rev.*, *99*, 125–161, doi:10.1016/j.earscirev.2010.02.004.

Seo, J., S. M. Kang, and D. M. W. Frierson (2014), Sensitivity of intertropical convergence zone movement to the latitudinal position of thermal forcing, *J. Clim.*, *27*, 3035–3042, doi:10.1175/JCLI-D-13-00691.1.

Sorteberg, A., and N. G. Kvamsto (2006), The effect of internal variability on anthropogenic climate projections, *Tellus, Ser. A*, *58*, 565–574.

St. Claire, S. B., E. A. Sudderth, M. L. Fischer, M. S. Torn, S. A. Stuart, R. Salve, D. L. Eggett, and D. D. Ackerly (2009), Soil drying and nitrogen availability modulate carbon and water exchange over a range of annual precipitation totals and grassland vegetation types, *Global Change Biol.*, *15*, 3018–3030.

Taylor, K. E., R. J. Stouffer, and G. A. Meehl (2012), An overview of CMIP5 and the experiment design, *Bull. Am. Meteorol. Soc.*, *93*, 485–498.

van der Molen, M. K., et al. (2011), Drought and ecosystem carbon cycling, *Agr. Forest Meteorol.*, *151*, 765–773.

Woollings, T. (2010), Dynamical influences on European climate: An uncertain future, *Philos. Trans. R. Soc. London, Ser. A*, *368*, 3733–3756.

Xie, S.-P., B. Lu, and B. Xiang (2013), Similar spatial patterns of climate responses to aerosol and greenhouse gas changes, *Nat. Geosci.*, *6*, 828–832.